Journal of Solid State Chemistry **158,** 180–186 (2001)
doi:10.1006/jssc.2001.9090, available online at http://www.idealibrary.com on IDEAL®

Preparation, Characterization, and Spectral Studies on Nanocrystalline Anatase TiO_2[1]

K. Madhusudan Reddy, C. V. Gopal Reddy, and S. V. Manorama[2]

Materials Science Group, Inorganic and Physical Chemistry Division, Indian Institute of Chemical Technology, Hyderabad 500 007, India

Received August 2, 2000; in revised form December 14, 2000; accepted January 19, 2001; published online March 27, 2001

Fine polycrystalline, nanoparticles of pure anatase titanium dioxide (average crystallite size ~3–10 nm) with high surface area (~210 m^2/g) have been synthesized in the pure anatase phase. Synthesized powder is characterized by DTA–TGA, FT–IR, XRD, BET surface area, SEM, TEM, and UV–Visible absorption spectroscopy. Polymer capping of the synthesized TiO_2 particles showed an improved stability against agglomeration and photo-degradation. The prepared nanoparticles showed a blue shift in the absorption spectra. Bandgap energy values observed for different particle sizes are 3.167 (3 nm), 3.145 (6 nm), and 3.027 eV (39 nm) for commercial TiO_2. TiO_2 is encapped with eriochromcyanin dye; the nanoparticles showed a noticeable shift in the acquired color toward the blue region with the decrease in the particle size. © 2001 Academic Press

Key Words: **nanoparticles; titanium dioxide; semiconductor; hydrolysis; bandgap; UV–Vis spectroscopy; quantum size effect.**

1. INTRODUCTION

As materials science and engineering evolves we are witnessing new approaches that provide increasingly precise control, at the atomic and molecular levels, over the structure, properties, and function of materials. Although this is largely driven by a recognition that familiar bulk properties—mechanical, magnetic, electronic, and optoelectronic—depend upon atomic and molecular building blocks, the same properties often differ from bulk when examined on the nanometer scale. Smallness in itself is not the goal. Instead, it is the realization, or now possibly even the expectation, that new properties intrinsic to novel structures will enable breakthroughs in a multitude of technologically important areas (1). The impact of nanostructure on the properties of high surface area materials is an area of increasing importance for understanding, creating, and improving materials for diverse applications.

A unique property of nanoparticulates is their extremely high surface area; they have many more sites for achieving property enhancements, making them ideal for a wide variety of applications. The synthesis of nanoparticles with controlled size and composition is of technological interest. The effort to understand the physics of ever-smaller structures has kept pace with attempts to exploit their beneficial properties. The phenomena of semiconductor nanocrystals showing size-tunable optical properties and metal nanoparticles that influence the activity and specificity of catalysis have been integrated into exploratory optical and electronic devices (2). In particular, there has been a lot of emphasis on the production of nanoparticles of TiO_2 for a wide variety of applications.

Synthetic routes for TiO_2 (titania or titanium dioxide) production usually result in titanium hydroxide, amorphous solid TiO_2 or crystallites, anatase, or rutile depending on the preparation route and experimental conditions. It is also known that the transformation behavior from the amorphous to the anatase or rutile phase is influenced by the synthesis conditions; however, most of the literature shows that alkoxide-based sol–gel or precipitation processes yield amorphous titania precursors or powders preferentially in the anatase phase (3–5).

The anatase phase of TiO_2, which is the stable phase at low temperatures, has gained importance as a photo-catalyst (6) for photodecomposition and solar energy conversion because of its high photoactivity (7, 8). TiO_2 shows different electrical characteristics with oxygen partial pressure, because it has wide chemical stability and a nonstoichiometric phase region. Because of this, it is suitable as a humidity sensor and high-temperature oxygen sensor (9–11). Furthermore, the properties of nanosized semiconductor particles have long been known to depend very sensitively on the particle size (12). As the diameter of crystallite approaches the exciton Bohr diameter, a splitting of the energy bands into discrete quantised energy level occurs. This is the so-called *quantum size effect*. Size quantization leads to a blue shift in the absorption spectrum due to increased bandgap, nonlinear optical properties, and unusual luminescence.

[1] IICT Communication No. 4594.

[2] To whom correspondence should be addressed. E-mail: manorama@iict.ap.nic.in.

0022-4596/01 $35.00

2. EXPERIMENTAL

2.1. Preparation of the Nanoparticles of Anatase TiO_2

Various synthesis methods such as hydrolysis (14), sol–gel (15–17), microemulsion or reverse micelles (18–21), and hydrothermal (22–25) synthesis have been used to prepare nanoparticles of titanium dioxide. Compared to other methods, hydrolysis could be carried out at conditions closer to ambient to produce nanoparticles of TiO_2. The nanocrystalline anatase titanium dioxide powders reported in this study were prepared by $TiCl_4$ hydrolysis. Titanium tetrachloride (98% $TiCl_4$) (Loba Chemie) was used as the starting material without any further purification. When $TiCl_4$ is dissolved in water, the heat of the exothermic reaction effects the formation of orthotitanic acid [$Ti(OH)_4$]. Since the formation of the species disturbed the homogenous precipitation, appreciated amount of $TiCl_4$ was initially digested in hydrochloric acid and then diluted in distilled water, all this while keeping the reaction vessel in an ice-water bath. The concentration of titanium tetrachloride was adjusted to 3 M in water. The initial pH was found to be about 1.8. A solution of hydrazine hydrate, H_6N_2O (Ranbaxy) in water (5 M) was added drop wise to the solution until the final pH was about 7.5 to 8.0. The hydrolysis and condensation reactions starts immediately upon mixing, as indicated by the rapid increase in turbidity and the formation of large, visible flocs, which precipitated to the bottom of the reaction vessel. The mixture was kept under high-speed constant stirring on a magnetic stirrer for 1 h at room temperature. Subsequently, the precipitated titanium dioxide ($TiO_2.nH_2O$) was filtered and repeatedly washed with hot distilled water to make $TiO_2.nH_2O$ free of chloride ions. The hydrous oxide was dried at 90–100°C over night and then ground to a fine powder. The polycrystalline titanium dioxide powders were then calcined at 100, 200, 300, 400, 500, or 600°C for 2 h to observe the phase changes accompanying the heat treatments.

Samples for UV–visible spectroscopy studies were prepared starting with various concentrations of $TiCl_4$, 0.1 M (Sample A) and 0.05 M (Sample B). Commercial TiO_2 from Aldrich (Sample C) was taken as reference. These three samples (each of 0.4 g TiO_2) were subsequently capped with 0.005 g of poly (ethylene glycol) (PEG) and sequentially labeled as Samples D, E, and F. All the samples were uniformly incorporated with 0.001 g eriochromcyanin dye. The samples appeared in different colors, which is attributed primarily to the particle size variation.

2.2. Nanoparticle Characterization

(*a*) *DTA–TGA.* The dried fine powder of synthesized TiO_2 was subjected to thermo gravimetric–differential thermal analysis (TG–DTA) (Mettler Toledo Star system). This was done to determine the temperatures of possible decomposition and phase changes. The samples were heated at the rate of 20°C/min and held at 200°C for 30 min and then the heating was resumed up to 1000°C.

(*b*) *XRD.* Powder X-ray diffraction (XRD) was used for crystal phase identification and estimation of the crystallite size. The X-ray Diffraction (XRD) measurements were performed on a Seimens/D5000 X-ray diffractometer. From the line broadening of corresponding X-ray diffraction peaks and using the Scherrer formula the crystallite size, L has been estimated (26)

$$L = K\lambda/(\beta \cos \theta),$$

where λ is the wavelength of the X-ray radiation (Cu$K\alpha$ = 0.15406 nm), K is a constant taken as 0.89, β is the line width at half maximum height, and θ is the diffracting angle.

(*c*) *Surface area.* The Brunauer–Emmett–Teller (BET) surface area was determined using a Micromeritics Pulse Chemisorb 2700 nitrogen adsorption apparatus. The samples were dried in a flow of inert gas (Helium) at 250°C and the surface area of the samples was estimated by N_2 chemisorption.

(*d*) *IR spectroscopy.* FT–IR studies were carried out in the 400–4000 cm^{-1} frequency range. For the infrared absorption spectra, the samples were formed into pellets with KBr and the spectra were recorded on a Nicolet740 FTIR Spectrometer at ambient conditions. IR spectroscopy in the transmission mode gives qualitative information about the way in which the adsorbed molecules are bonded to the surfaces as well as the structural information of solids.

(*e*) *SEM and TEM analysis.* The samples calcined at 400°C were dispersed in distilled water and then sonicated ultrasonically to separate out individual particles, for the determination of the particle size. The particle size and external morphology of the samples were observed on a Hitachi S520 scanning electron microscope (SEM) and transmission electron micrographs (TEM) were recorded on a JEOL JEM-100CX electron microscope.

(*f*) *UV–visible absorption spectrum.* The samples were dispersed in distilled water and sonicated ultrasonically for the absorption studies on a Shimadzu 240 (Japan) spectrophotometer. The quantum size effect is better understood from the UV absorption spectra. The absorption spectra also give an estimate of the size distribution in the sample from the sharpness of the absorption features. The salient features of the absorption spectra can be clearly deciphered from the second derivative spectra (13). The position of the minima in the second derivative spectra gives a good approximation of the position of the shoulders that arise from the transitions to discrete higher electronic levels.

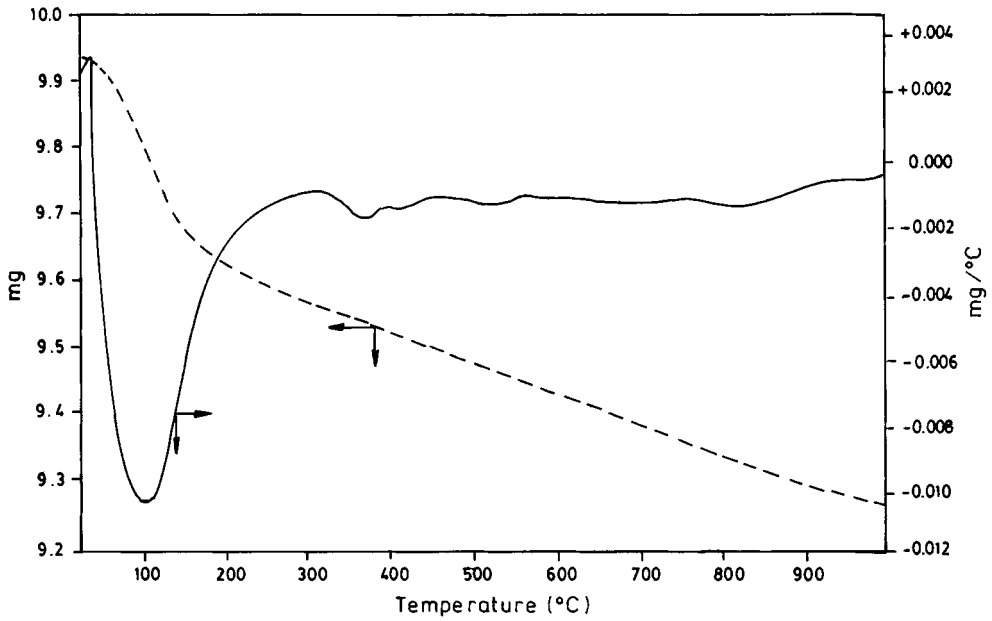

FIG. 1. DTA–TGA curve of prepared nanocrystalline TiO_2: (—) DTA, (. . .) TGA.

3. RESULTS AND DISCUSSION

3.1. DTA–TGA

Figure 1 shows the typical DTA and TGA thermodiagrams for the as prepared product. DTA analysis of the product indicates a prominent endotherm below 100°C due to free adsorbed water. The exothermic shoulder around 300°C corresponds to the decomposition of residual –OH groups and the condensation of nonbonded oxygen. The process continues with an exothermic peak at about 390°C, which corresponds to the crystallization of the anatase phase. At 560°C the product completely transforms into the anatase phase. At around 700°C the rutile phase starts appearing. Thereafter no significant thermal effects can be detected even up to 1000°C.

3.2. FT–IR

Figure 2 (lines a and b) shows the spectra of prepared and poly(ethylene glycol) (PEG) capped TiO_2, respectively. Figure 2 (line a) shows the IR spectrum of the TiO_2 in the range of 400–4000 cm^{-1}, which agrees with the reported data (27). Figure 2 (line b) is for the polymer capped TiO_2. The bifurcated peak between 2800 and 2900 cm^{-1} is due to alkyl group of poly(ethylene glycol). The broad peak at 1100 cm^{-1} is that of the ether linkage ($-CH_2-O-CH_2-$) and the peak between 3200 and 3600 cm^{-1} suggests the presence of hydroxyl groups in diblock at one terminal. This data shows that TiO_2 has been effectively capped with poly(ethylene glycol).

3.3. XRD

Figure 3 (lines a–g) shows the XRD patterns of samples as synthesized and subsequently calcined at different

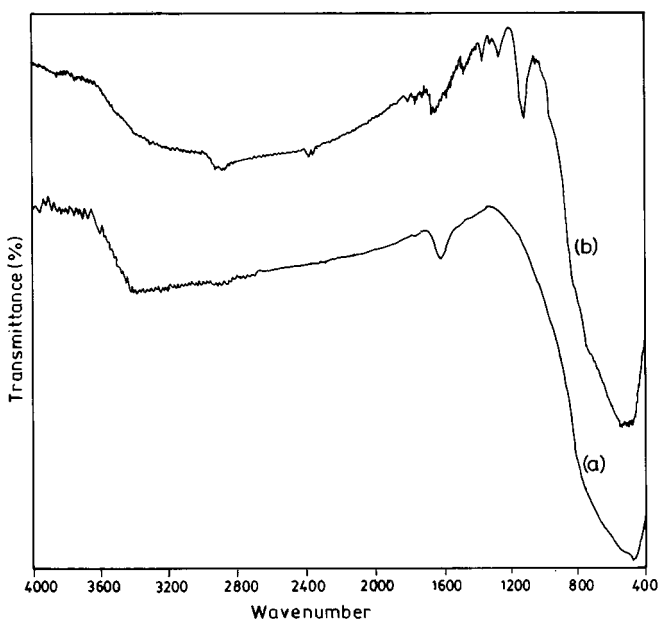

FIG. 2. FT–IR spectrum of (a) nanocrystalline TiO_2 and (b) nanocrystalline TiO_2 capped with PEG.

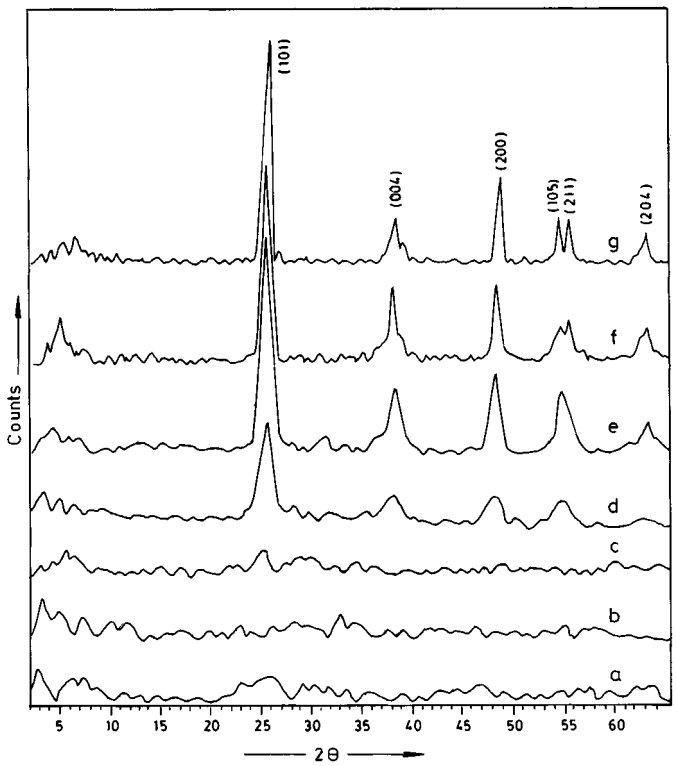

FIG. 3. XRD pattern of TiO_2 calcined at (a) RT, (b) 100°C, (c) 200°C, (d) 300°C, (e) 400°C, (f) 500°C, and (g) 600°C.

temperatures from 100 to 600°C. The as-prepared sample is largely amorphous. Calcination is a common treatment used to improve the crystallinity of TiO_2 powders. When TiO_2 powders were calcined at higher temperatures, the transformation such as amorphous to anatase phase occurs. The amorphous–anatase transformation was complete in the temperature range from 400 to 600°C as is evident from the figure. The XRD peaks of powder calcined at 100, 200, or 300°C are weak in comparison to those of the samples calcined at higher temperatures, which suggests that a significant amount of amorphous phase still remains in the powder at these temperatures. The crystallite size was estimated by the Scherrer formula (26), which is generally the accepted method to estimate the mean crystallite size. The crystallite sizes were found to be in nanometer regime 6.1, 8.07, 8.50, and 12.10 nm for the samples calcined at 300, 400, 500, or 600°C respectively. The XRD patterns of the amorphous TiO_2 are in agreement with those reported (28), so the effect of the amorphous material on the broadening of the XRD patterns of nanosized TiO_2 is negligible. There is also a report by Sunstrom *et al.* (29) with a similar XRD pattern for TiO_2 prepared by the hydrodynamic cavitation method. The particle size calculations were made from the TEM micrographs and were found to be around 3–8 nm. The particle size is uniform as seen from the micrographs in Figs. 4a and 4b.

3.4. Surface Area

The surface area measurements were carried out for nanoparticles of TiO_2 calcined at temperatures from 100 to 600°C. The as-prepared sample showed a BET surface area of 213 m^2/g and the one calcined at 600°C, 65 m^2/g. The results of surface area measurements and the crystallite size are depicted in Fig. 5.

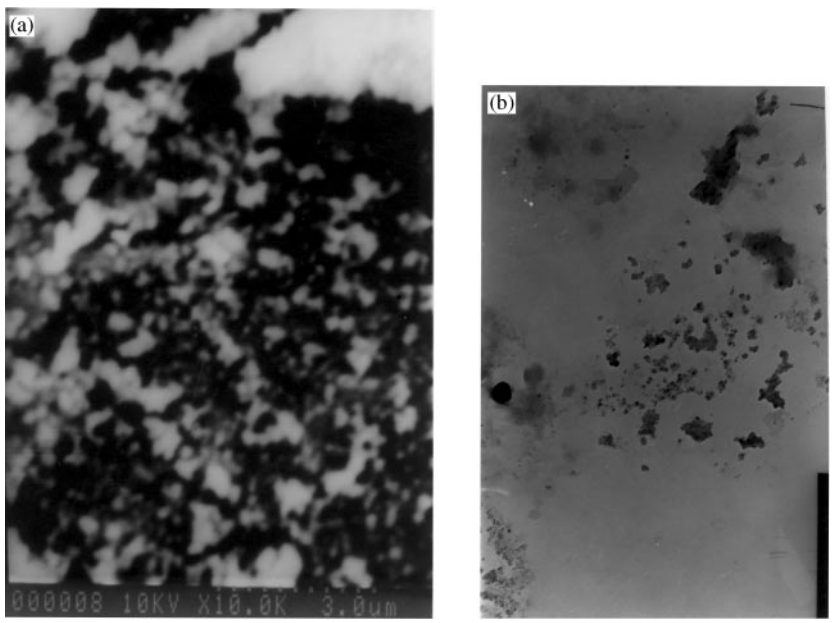

FIG. 4. Typical (a) scanning electron (× 10K) and (b) transmission electron (× 20K) micrographs of the synthesized TiO_2.

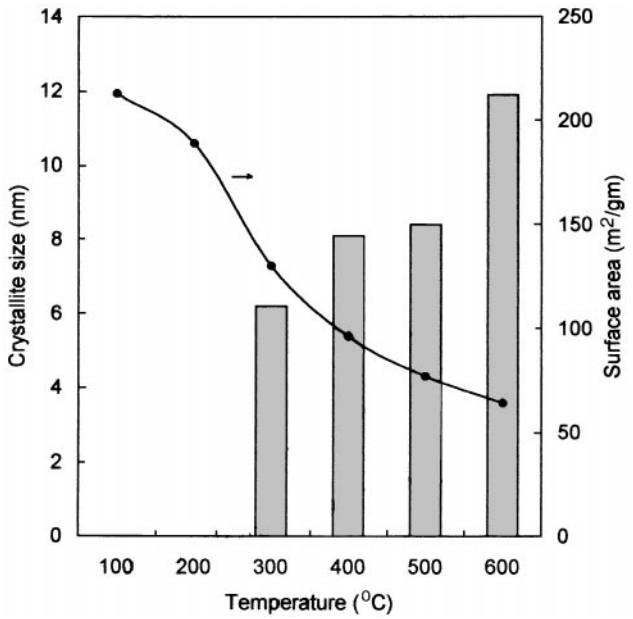

FIG. 5. Variation of the crystallite size and surface area as a function of the calcination temperature of TiO_2.

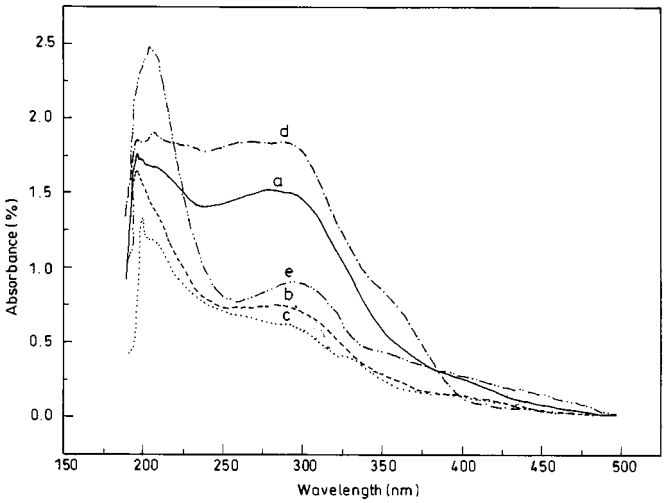

FIG. 6. UV–vis absorption spectra of TiO_2 showing the blue shift with decrease in particle size (a) 0.1 M ($E_g = 3.145$ eV), (b) 0.05 M ($E_g = 3.167$ eV), (c) commercial TiO_2 ($E_g = 3.027$ eV), (d) 0.1 M ($E_g = 3.145$ eV) capped with PEG, and (e) 0.05 M ($E_g = 3.167$ eV) capped with PEG.

3.5. Quantum Size Effect of the TiO_2 Nanoparticles from UV–Vis Spectroscopy

UV–vis spectroscopy has been used to characterize the bulk structure of crystalline and amorphous titanium dioxide. Titania is a semiconducting oxide with easily measured optical bandgap. UV–vis diffuse reflectance spectroscopy is used to probe the band structure or molecular energy levels in the materials since UV–vis light excitation creates photo-generated electrons and holes. The UV–vis absorption band edge is a strong function of titania cluster size for diameters less than 10 nm, which can be attributed to the well-known quantum size effect for semiconductors (30). Figure 6 (lines a–e) shows the UV–visible absorption spectra of the sample (a) 0.1 M, (b) 0.05 M, (c) commercial, (d) 0.1 M with PEG capped, and (e) 0.05 M with PEG capped titania nanoparticles. The M indicates the molarity of the starting material, titanium tetrachloride. When the concentration of starting material is varied, the absorption spectra of the synthesized nanoparticles show a difference. Extrapolating the curves in the plot we have the bandgap energy of the nanoparticles. The bandgap energies (E_g) obtained are as follows: for the 0.1 M samples, it is 3.145 eV (absorption edge at about 395 nm), for the 0.05 M samples, it is 3.167 eV (absorption edge at 392 nm), and for (c) the commercial sample the value is 3.027 eV (absorption edge is at 404 nm). It is clear that as the particle size decreases the bandgap energies increase. Size quantization causes the absorption edge to be shifted to higher energies. From the shift in the bandgap (ΔE_g), the particle size can be approximated using Eq. [1]. The samples obtained from 0.1 M titanium tetrachloride have an average particle size of 6 nm and those from 0.05 M titanium tetrachloride average about 3 nm.

The optical absorption threshold for nanocrystallites of this size shifts to higher energies, i.e., toward the blue end of the spectrum as the crystallite size decreases (31). The size-dependent shift in the bandgap can be calculated as

$$\Delta E_g = \hbar^2\pi^2/2R^2\ \{1/m_e + 1/m_h\} - 1.786\ e^2/\varepsilon R\ (0.248\ E_{RY}), \quad [1]$$

where R, is the radius of the particle and E_{RY}, is the effective Rydberg energy. This model predicts an increase in the bandgap with decrease in particle dimensions. The size-dependent shift in the bandgap is found to be 0.1–0.2 eV (32).

The nature of the absorption spectra can be more clearly seen from the second derivative spectra. Figure 7 (lines a–e) shows the double derivative of the absorption spectra of the samples replotted using the data of Fig. 6. The position of the minima in the double derivative gives a good approximation of the position of the shoulders of the absorption spectra. These shoulders arise from the transitions to discrete higher electronic levels. The energies required for the higher transitions gradually increase with decreasing particle size. This can be visualized from Fig. 7. Since the particle size of the sample (b) is 3 nm, the position of the minima is toward the lower wavelength (higher energy) compared with sample (a), which has particle size of 6 nm

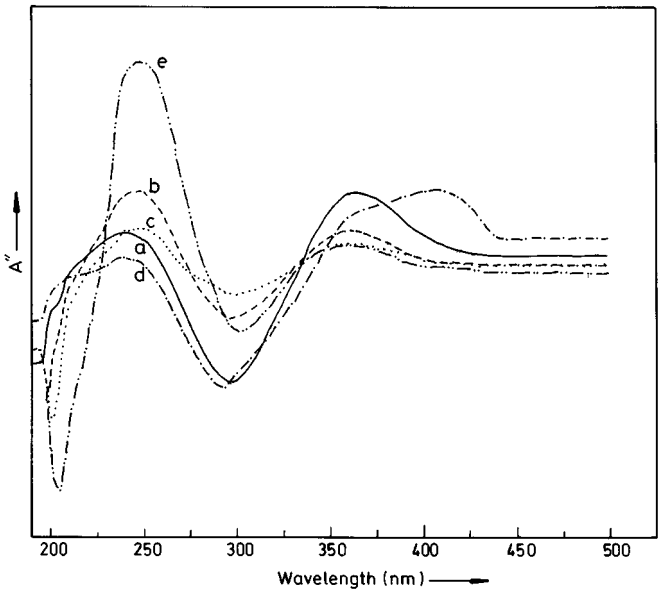

FIG. 7. Second derivative of UV–vis absorption spectra of TiO_2 nanoparticles showing the position of shoulders, replotted using Fig. 6.

and has the minima toward higher wavelength. It is observed that the energies required for the higher transitions gradually increase with decreasing particle size, in agreement with the theoretical predictions (13).

3.6. *Effect of Polymer Capping on TiO_2 Nanoparticles*

Figure 8 (I and II) shows the UV–visible absorption spectrum for the nanoparticles of titanium dioxide (with and without polymer capping). In Fig. 8(I), the curves A and B give the absorption spectra of nanoparticles of TiO_2: (A) for the particles synthesized from the 0.1 M solution, (B) for the particles synthesized from 0.05 M solution of $TiCl_4$. The curves A48 and B48 give the absorption spectra of the samples A and B taken after 48 h. The observed shift in the absorption spectra of the latter samples can be attributed to the agglomeration of the nanoparticles with time. Figure 8(II) shows the absorption spectra of the samples with polymer–capped nanoparticles of TiO_2. Spectra D and E are for the samples A and B capped with the polymer PEG correspondingly. In this latter case we observed that even though we recorded the absorption spectra after 48 h there is not much difference in the intensities nor is there any shift. The two spectra nearly overlap. This is as expected, since the PEG capping of the nanoparticles prevents agglomeration of the particles. The polymer acts as a barrier between the particles and prevents any kind of interaction between them.

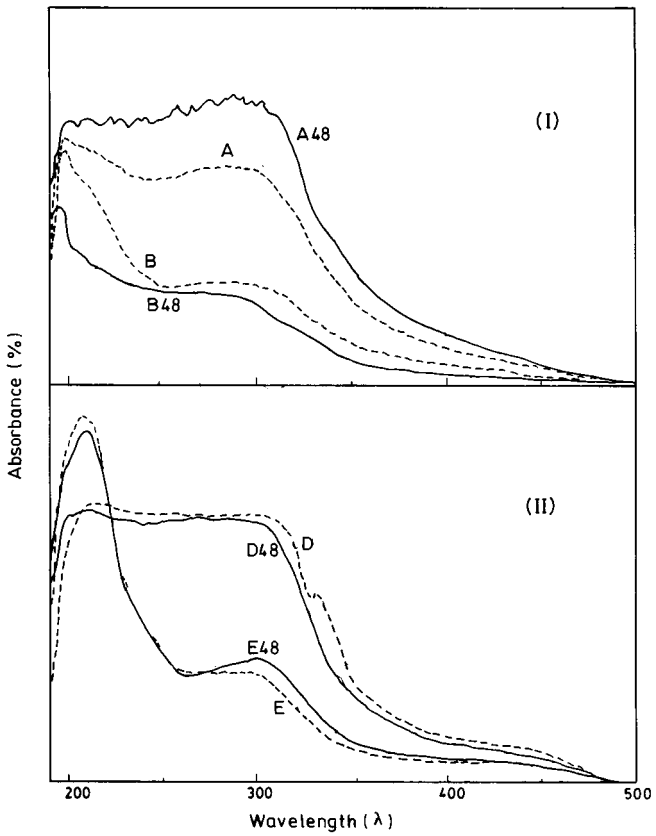

FIG. 8. (I) UV–vis spectra of (A) 0.1 M and (B) 0.05 M TiO_2 nanoparticles and (A48) 0.1 M and (B48) 0.05 M TiO_2 nanoparticles after 48 h. (II) UV–vis spectra of PEG-capped (D) 0.1 M and (E) 0.05 M TiO_2 nanoparticles, and PEG-capped TiO_2 (D48) 0.1 M, (E48) 0.05 M stabilized after 48 h.

3.7. *Incorporation of Dye*

All of the samples are incorporated with 0.001 g of eriochromcyanin. The prepared nanocrystalline sample 0.1 M gave pink color and the sample with 0.05 M gave light orange. The photographs show a distinct color change with the change in the size of the particle. Since the particles prepared from 0.05 M solution of $TiCl_4$ are comparatively smaller than those prepared from 0.1 M solution the color pattern shows a blue shift: from pink to light yellow. This indicates a shift in the color toward the blue region.

4. CONCLUSIONS

The results presented in this paper bring out the following conclusions:

- A method for preparation of TiO_2 nanoparticles with large surface area and exclusively anatase crystal structure has been demonstrated.

- Successfully characterized, the synthesized particles in the nanometre regime and the size of the crystals were found to be 3–10 nm as estimated from Scherrer formula. This data is also supported by evidence from SEM and TEM micrographs.
- The TiO_2 synthesized has a large surface area, 210 m^2/g as estimated by the BET method and this is a very important property for catalytic, photocatalytic, and gas sensor applications.
- The nanoparticles showed a concomitant blue shift in the absorption spectrum with a decrease in the particle size.
- The bandgap energy values observed for different particle sizes were 3.167 eV (3 nm), 3.145 eV (6 nm) for prepared TiO_2 and 3.027 eV (39 nm) for commercial titanium dioxide. These shifts are in good agreement with the calculated values.
- Eriochromcyanin-incorporated nanoparticles differed in color with the change in particle size.
- The TiO_2 capped with PEG restricted the agglomeration of the particles.

REFERENCES

1. R. W. Siegel, *Ann. Rev. Mater. Sci.* **21,** 559 (1991).
2. R. P. Andres, T. Bein, M. Dorogi, S. Feng, J. I. Henderson, C. P. Kubiak, W. Mahoney, R. G. Osifchin, and R. Reifenberger, *Science* **272,** 1323–1325 (1996).
3. J. Y. Chen, L. Gao, and J. H. Huang, *J. Mater. Sci.* **31,** 3497 (1996).
4. D. C. Hague and M. J. Mayo, *J. Am. Ceram. Soc.* **77,** 1957–1960 (1994).
5. K.-N. P. Kumar, K. Keizar, A. J. Burggaraaf, T. Okubo, H. Nagamoto, and S. Morooka, *Nature* **358,** 48–51 (1992).
6. A. Fujishima and K. Honda, *Nature* **238,** 37–38 (1972).
7. A. Larson and J. L. Falconer, *Appl. Catal. B* **4,** 325–342 (1994).
8. P. V. Kamat and N. M. Dimitrijevic, *Solar Energy* **44**(2), 83–89 (1990).
9. L. Micheli, *Am. Ceram. Soc. Bull.* **54,** 694–698 (1984).
10. K. L. Siefering and G. L. Griffin, *J. Electrochem. Soc.* **137**(3), 814–818 (1990).
11. H. Tang, K. Prasad, R. Sanjjiness, and F. Levy, *Sens. Actuators B* **26–27,** 71–75 (1995).
12. G. Schmid, M. Baumle, M. Greekens, I. Heim, C. Osemann, and T. Sawitowski, *Chem. Soc. Rev.* **28,** 179–185 (1999).
13. M. Sequeira and S. G. Dixit, *Chemical Industry Digest*, March/April p. 60 (1999).
14. V. Chhabra, V. Pillai, B. K. Mishra, A. Morrone, and D. O. Shah, *Langmuir* **11,** 3307–3311 (1995).
15. M. Lal, V. Chhabra, P. Ayyub, and A. Maitra, *J. Mater. Res.* **13**(5), 1249 (1988).
16. L. K. Campbell, B. K. Na, and E. I. Ko, *Chem. Mater.* **4**(6), 1329–1333 (1992).
17. U. Selvaraj, A. V. Prasadrao, S. Komerneni, and R. Roy, *J. Am. Ceram. Soc.* **75**(5), 1167–1170 (1992).
18. T. Sugimoto, K. Okada, and H. Itoh, *J. Colloid. Interface Sci.* **193,** 140 (1997).
19. H. Kumazava, H. Otuski, and E. Sada, *J. Mater. Sci. Lett.* **12,** 839–841 (1993).
20. R. R. Basca and M. Gratzel, *J. Am. Ceram. Soc.* **79**(8), 2185–2188 (1996).
21. H. Cheng, J. Ma, Z. Zhao, and L. Qi, *Chem. Mater.* **7,** 663–667 (1995).
22. T. R. N. Kutty, R. Vivekanandan, and P. Murugaraj, *Mater. Chem. Phys.* **19**(6), 533–546 (1988).
23. Y. Qian, Q. Chen, Z. Chen, C. Fan, and G. Zhou, *J. Mater. Chem.* **3**(2), 203–205 (1993).
24. T. Masui, K. Fujiwara, K. Machida, and G. Adachi, *Chem. Mater.* **9**(10), 2197 (1997).
25. E. Stathatos, P. Lianos, F. Del Monte, D. Levy, and D. Tsiourvas, *Langmuir* **13,** 4295–4300 (1997).
26. B. D. Cullity, "Elements of X-Ray Diffraction." Adison-Wesley, Reading, MA, 1978.
27. R. A. Nyquist and R. O. Kagel, "IR Spectra of Inorganic Compounds." Academic Press, New York, 1971.
28. S.-J. Kim, S.-D. Park, Y. H. Jeong, and S. Park, *J. Am. Ceram. Soc.* **82**(4), 927–932 (1999).
29. J. E. Sunstrom IV, W. R. Moser, and B. Marshik-Guerts, *Chem. Mater.* **8**(8), 2061–2067 (1996).
30. M. Anpo, T. Shima, S. Kodama, and Y. Kobokawa, *J. Phys. Chem.* **91,** 4305–4310 (1987).
31. M. A. Reed, *Scientific American*, January, p. 99 (1993).
32. S. V. Manorama and K. Madhusudan Reddy, *Appl. Phys. Lett.*, submitted.